SME Annual Meeting
Feb. 27 - Mar. 02, 2022, Salt Lake City, UT

Preprint 22-096

WAVELENGTH SELECTIVE PORTABLE DEVICE FOR QUANTIFYING ORGANIC AND ELEMENTAL CARBON IN DIESEL PARTICULATE MATTER

D. A. Parks, CDC NIOSH, Spokane, WA
K. V. Raj, CDC NIOSH, Spokane, WA
A. T. Weakley, Weakley Consulting, Sacramento, CA
A. L. Miller, Miller Consulting, Spokane, WA

ABSTRACT

Diesel particulate matter (DPM) is a common and well-known health hazard in the mining environment. The current approved method for monitoring both the organic and elemental carbon (OC, EC) portions of DPM is a laboratory method with a turnaround time of approximately one week. In order to evaluate exposure levels and take corrective action before overexposures occur, a portable real-time device capable of quantifying both OC and EC is needed. To that end, researchers from the National Institute for Occupational Safety and Health (NIOSH) designed and tested a device based on narrow bandpass optical filters that is capable of targeting infrared absorbance bands associated with DPM. Five optical bandpass filters were chosen based on previous work quantifying DPM using Fourier-transform infrared (FT-IR) spectrometry. The resulting device, referred to as a filtometer, is optimized to exclusively determine DPM and could serve as a cost-effective, field-portable alternative to laboratory-grade FT-IR analysis and instrumentation. The performance of the filtometer was investigated by calibrating FT-IR data from DPM (dependent variable) to the filtometer spectra (predictor variables) using a partial least-squares (PLS) and ordinary least squares (OLS) approach. The square of the correlation coefficient and root-mean-square error of cross validation measures were used to assess individual model performance.

INTRODUCTION

Diesel particulate matter (DPM) has been classified as carcinogenic to humans [1]. Due to the negative health effects of exposure to high levels of DPM, the Mine Safety and Health Administration (MSHA) regulates exposure at the permissible exposure limit (PEL) of 160 µg/m^3 over a regular working shift (8 hours). The approved method for determining DPM exposure requires drawing the mine air through a quartz fiber filter using personal sampling equipment, packaging and shipping filters to a laboratory for analysis, and measuring the collected mass using thermal optical carbon analysis (*i.e.*, NIOSH method 5040) [2]. A time-weighted average of DPM concentration may then be derived and compared to the PEL [3].

Devices which quantify DPM in a timelier manner aim to prevent overexposures in the evolving mining environment. Several devices on the market utilize light absorption or scattering in the UV to near-infrared region of the electromagnetic spectrum to quantify DPM. However, the fundamental molecular absorption bands characteristic of DPM, which allow for chemical speciation and accurate quantification, occur in the mid-infrared region [4]. Since the currently available devices do not interrogate the mid-infrared region, they require aerosol-specific calibrations in order to accurately quantify both organic carbon (OC) and elemental carbon (EC) [5-9]. The aim of this work is to validate the components which could be used in a portable real-time device to quantify both the organic (OC) and elemental (EC) fractions of DPM.

Previous work at NIOSH has demonstrated that diffuse reflectance Fourier-transform infrared spectrometry (FT-IR) is can quantify both the OC and EC fractions of DPM in particulate matter collected on quartz fiber filters [10]. This work demonstrates a simple device, sometimes known as a filtometer [11], can quantify DPM OC and EC using five optical bandpass filters to sample regions of the mid-infrared.

Specifically, infrared radiation is provided by way of a flash bulb driven with a 50 Hz square wave. A thermoelectrically-cooled mercury cadmium telluride (MCT) detector measures the transmitted infrared radiation that passes through the DPM-laden filter and each of the five passband filters in turn. The detector output is then passed through a preamplifier and then to a digital oscilloscope where it is averaged over 512 cycles and the peak-to-peak waveform amplitude recorded. The result is a sparse low-resolution absorption spectrum of DPM. Polystyrene is a common standard used to calibrate infrared spectrometers and was therefore used to check filtometer performance. Figure 1 shows transmission FT-IR spectrum of a polystyrene standard overlain with the filtometer spectrum

Figure 1 illustrates that the filtometer produces a sparse low-resolution spectrum directly related to the FT-IR spectrum (see Appendix for a theoretical treatment of the described relationship). Clearly considerable information is lost when a filtometer is used in place of an FT-IR spectrometer. However, the filtometer's passband filters were deliberately chosen to collect infrared absorption germane to OC and EC quantification.

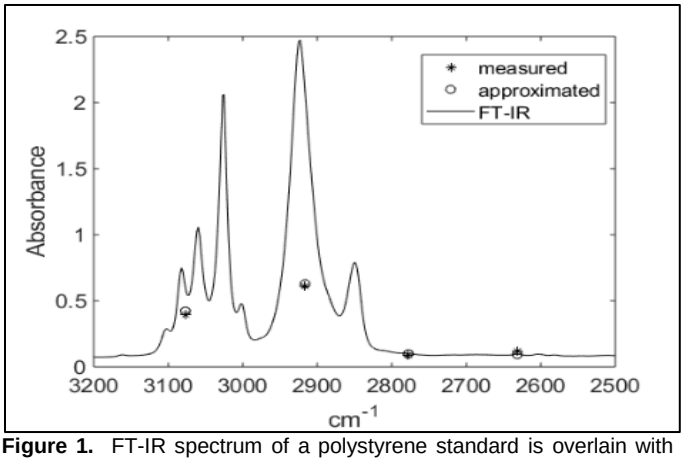

Figure 1. FT-IR spectrum of a polystyrene standard is overlain with the measured filtometer spectrum (*) as well as a theoretical approximation of the FT-IR spectrum (o), calculated to estimate filtometer performance (see Appendix for details). Note that the highest wavelength sampled by the filtometer is outside the range of the FT-IR instrument and therefore not shown here.

The benefit of utilizing this filtometer therefore lies in reducing processing time costs by having a real-time DPM quantification, as well as the ability to miniaturize infrared sampling, which will also help timely decision making to reduce worker exposure. Although near-infrared spectrometers have been miniaturized to an extent commensurate with a belt wearable device [12], this has yet to be

achieved for mid-infrared spectrometers where information related to OC and EC is found.

Over a hypothetical 8-hour shift with DPM concentrations at the permissible exposure limit (PEL), we would expect 16 µg/cm^2 on the quartz fiber filter when standard sampling methods are adhered to. The standard sampling method utilizes a 1.7 lpm pump and a submicron impactor to deposit the DPM onto a quartz fiber filter with an effective deposition area of 8 cm^2.

The resulting absorbance peak from ~16 ug/cm^2 OC is not as large as that of polystyrene but nonetheless visible in the filtometer spectrum as shown in Figure 2.

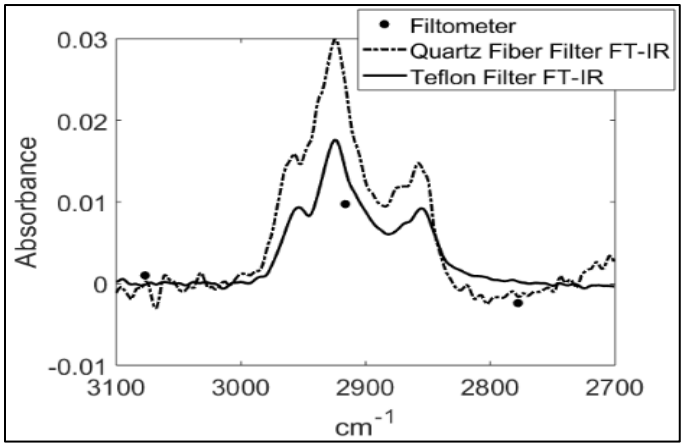

Figure 2. Aliphatic CH absorption bands of DPM OC measured by FT-IR spectrometry and the filtometer. The filtometer spectrum is compared to DPM OC measured from a quartz and Teflon filter sampled in parallel to ensure identical DPM deposition on each filter type. Spectra have been baseline corrected using a second order polynomial to facilitate comparison.

DPM SAMPLE GENERATION AND SAMPLE COLLECTION

The DPM samples used in this study were generated using a diesel generator coupled to a variable resistive load bank [10]. The variable resistive load bank alters the ratio of EC to OC by increasing engine load results in a greater relative amount of EC [13]. Using a multiport quiescence chamber, parallel samples are drawn through both quartz fiber and Teflon filters simultaneously to ensure equivalent mass loading. A total of 13 Teflon and quartz filter pairs were generated for quantitative analysis.

INFRARED ANALYSIS AND DPM CALIBRATION

The quartz fiber filters scatter too much infrared radiation and must be analyzed with the FT-IR in diffuse reflection mode. Teflon filters were utilized for the filtometer device so that it could operate in transmission mode. The Teflon filters are first analyzed using the five channel filtometer instrument. The passband filters are summarized in Table 1 and chosen to represent the bands used in [10] to quantify OC and EC. The diffuse-reflectance FT-IR spectra of quartz fiber filters are collected and OC and EC deposition measured (µg/cm^2) according to procedures developed in [10]. Filtometer spectra are then calibrated to parallel measurements of OC and EC deposition using an ordinary and partial least squares regression to provide filtometer-equivalent DPM OC and EC.

Table 1. Passband filters used in the filtometer.

Filter	Center [cm^{-1}]	Upper cutoff [cm^{-1}]	Lower cutoff [cm^{-1}]	Width [cm^{-1}]
1	3,077	3,030	3,125	95
2	2,916	2,858	2,977	119
3	2,778	2,743	2,813	69
4	4,049	4,008	4,090	82
5	2,632	2,618	2,646	28

Filtometer OC and EC were judged against the reference (a.k.a., FT-IR) OC and EC measurements using the root-mean-square error of leave-one-out cross validation (RMSECV) and squared correlation coefficient (r^2). Leave-one-out cross validation was also used to determine the optimal number of PLS components. Note that cross-validation was used in lieu of validating using an independent test set as samples were too few (N=14) to reliably partition into a training and test set.

RESULTS

This section presents the graphs of OC and EC estimation for both PLS and ordinary least squares (OLS) regression. The figures of merit RMSECV and r^2 are also provided.

The RMSECV was calculated by way of a leave-one-out cross validations scheme. This calculation involves using all *N* samples except for one, for example sample *j,* and performing OLS or PLS regression. The resulting model derived from the *N-1* samples is then used to calculate the OC and EC of sample *j,* that is $\widehat{OC}_j$ and $\widehat{EC}_j$. This process is repeated while leaving each sample out in turn.

The RMSECV is then calculated for OC as

$$RMSECV(OC) = \sqrt{\frac{1}{N}\sum_{j=1}^{N}\left(OC_j - \widehat{OC}_j\right)^2}$$

where OC_j is the OC as determined from the FT-IR spectrum [14]. The same process is performed for EC, the results of these two calculations are provided in Table 2.

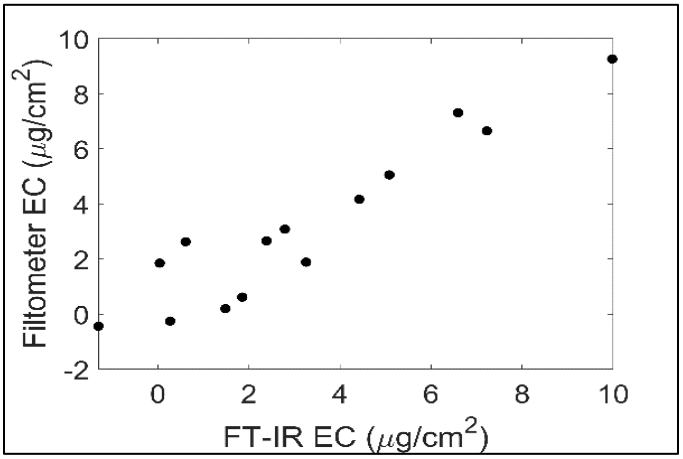

Figure 3. EC estimation using ordinary least squares regression on all 5 passband filters.

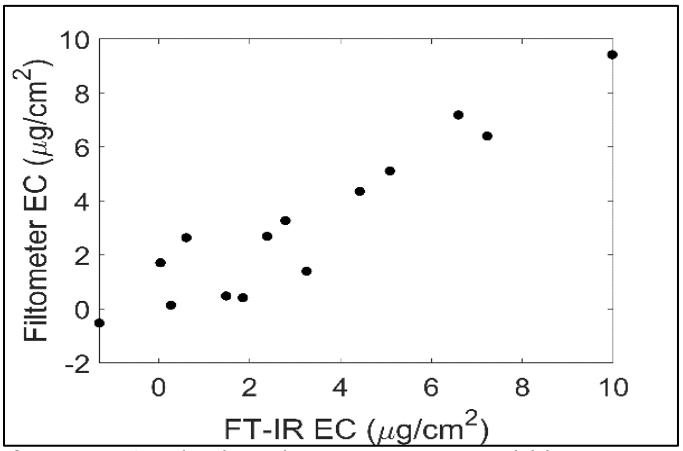

Figure 4. EC estimation using a 4-component partial least-squares regression on all 5 passband filters.

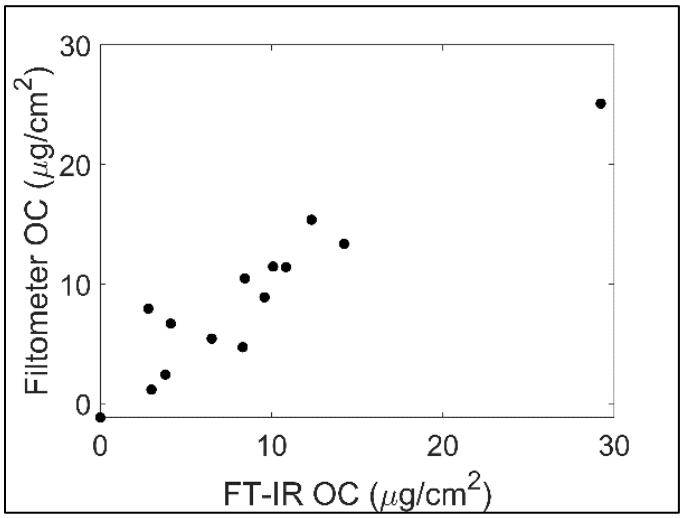

Figure 5. OC estimation using ordinary least squares regression on all 5 passband filters.

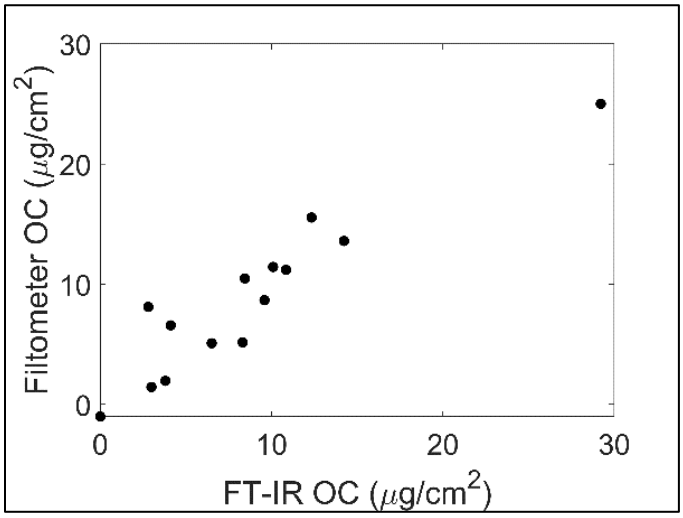

Figure 2. OC estimation using a 4-component partial least-squares regression on all 5 passband filters.

Table 2. RMSECV and r^2.

DPM component	*Model*	*RMSECV [µg/cm^2]*	*r^2*
EC	*OLS*	*1.9*	*0.88*
EC	*PLS*	*1.7*	*0.88*
OC	*OLS*	*5.0*	*0.87*
OC	*PLS*	*4.5*	*0.87*

CONCLUSION

A 2009 study on exposure to DPM in industries with a high reliance on diesel technologies found that underground mining was the industry wherein exposures were the highest [15]. Current methods for monitoring DPM with a compact real-time device require aerosol-specific calibrations [5-9]. A device operating in the mid-infrared region of the electromagnetic spectrum has the unique ability to identify specific molecular species [4] using their fundamental vibration and thus would eliminate the need for an aerosol specific calibration.

Having previously established that mid-infrared Fourier transform spectroscopy can quantify OC and EC as measured by the NIOSH 5040 method [10], a natural next step, namely testing infrared instrumentation conducive to a belt-wearable device, was carried out in this work. The instrumentation took the form of what is sometimes referred to as a filtometer [11]. The filtometer device was shown to be capable of estimating OC and EC reasonably accurately with a root mean square (RMS) error of 1.6 µg/cm^2 EC and 5 µg/cm^2 OC.

The use of a filtometer based device in place of an FT-IR or the thermal optical method would enable significantly smaller form factor thus allowing workplace exposure to DPM to be minimized by quantifying DPM concentration in a timely and portable manner. The introduction of next generation diesel technologies is leading to DPM composition showing a significantly larger portion of OC compared to that generated by older diesel technologies. Thus, the ability of the filtometer device to quantify OC is of great benefit to the mining workforce.

A filtometer is lacking in resolution as it samples the infrared spectrum at far few wavelengths than benchtop spectrometers. This in turn implies that filtometers are less flexible and in general are designed for specific applications. However, the number of specific applications are quite broad and thus other airborne hazards in the mining industry may potentially be quantifiable by way of the filtometer approach.

DISCLAIMER

The findings and conclusions in this paper are those of the authors and do not necessarily represent the official position of the National Institute for Occupational Safety and Health, Centers for Disease Control and Prevention.

REFERENCES

1. Benbrahim-Tallaa, L., R.A. Baan, Y. Grosse, B. Lauby-Secretan, F. El Ghissassi, V. Bouvard, N. Guha, D. Loomis, and K. Straif, Carcinogenicity of diesel-engine and gasoline-engine exhausts and some nitroarenes. The Lancet Oncology, 2012. 13(7): p. 663-664.
2. NIOSH, Diesel Particulate Matter (as Elemental Carbon), in NIOSH Manual of Analytical Methods (NMAM), . 1998.
3. Birch, M.E., Occupational monitoring of particulate diesel exhaust by NIOSH method 5040. Appl Occup Environ Hyg, 2002. 17(6): p. 400-5.
4. Griffiths, P.R. and J.A. de Haseth, Fourier transform infrared spectrometry. 2nd ed. 2007, Hoboken, NJ: John Wiley & Sons.
5. Khan, M.U., K.O. Homan, S.A. Saki, M.Z. Emad, and M.A. Raza, Real-time diesel particulate matter monitoring in underground mines: Evolution and applications. International Journal of Mining, Reclamation and Environment, 2020: p. 1-15.
6. Northrop, W.F., D. Zarling, and X. Li. Considerations in Using Photometer Instruments for Measuring Total Particulate Matter Mass Concentration in Diesel Engine Exhaust. in ASME 2017 Internal Combustion Engine Division Fall Technical Conference. 2017.
7. Robinson, M., Z.G. Liu, M. Olson, and J. Schauer, Comparison of Measurement Strategies for Light Absorbing Aerosols from Modern Diesel Engines. SAE International Journal of Fuels and Lubricants, 2014. 7(2): p. 543-550.
8. Watts, W.F., D.D. Gladis, M.F. Schumacher, A.C. Ragatz, and D.B. Kittelson, Evaluation of a Portable Photometer for Estimating Diesel Particulate Matter Concentrations in an Underground Limestone Mine. The Annals of Occupational Hygiene, 2010. 54(5): p. 566-574.
9. Miller, A.L., M.C. Habjan, and K. Park, Real-time estimation of elemental carbon emitted from a diesel engine. Environmental science & technology, 2007. 41(16): p. 5783-5788.
10. Parks, D.A., P.R. Griffiths, A.T. Weakley, and A.L. Miller, Quantifying elemental and organic carbon in diesel particulate matter by mid-infrared spectrometry. Aerosol Science and Technology, 2021: p. 1-14.
11. Wilks, P., ed. Infrared Filtometers. Handbook of Vibrational Spectroscopy, ed. J.M. Chalmers and P.R. Griffiths. 2001, John Wiley & Sons,: Chinchester, UK.

12. Beć, K.B., J. Grabska, H.W. Siesler, and C.W. Huck, Handheld near-infrared spectrometers: Where are we heading? NIR news, 2020. 31(3-4): p. 28-35.

13. McLaughlin, R.P., D.A. Parks, A.I. Grubb, G.S. Mason, and A.L. Miller, A predictive model for elemental carbon, organic carbon and total carbon based on laser induced breakdown spectroscopy measurements of filter-collected diesel particulate matter. Spectrochimica Acta Part B: Atomic Spectroscopy, 2020. 168: p. 105871.

14. Kalivas, J.H. and P.J. Gemperline, Calibration, in Practical Guide to Chemometrics, P.J. Gemperline, Editor. 2006, CRC/Taylor & Francis: Boca Raton, FL.

APPENDIX

The output from the detector after amplification as measured with a 1 MΩ input impedance oscilloscope can be written as

$$O_{open\ beam} = \int_0^{\infty} R(\lambda) * T_{passband}(\lambda) d\lambda \cong \int_{\lambda_1}^{\lambda_2} R(\lambda) d\lambda \quad \text{Equation 1}$$

where $R(\lambda)$ is the system response including the source, detector, and pre-amp characteristics. With the sample in the beam

$$O_{sample} = \int_0^{\infty} R(\lambda) * T_{sample}(\lambda) * T_{passband}(\lambda) d\lambda \cong \int_{\lambda_1}^{\lambda_2} R(\lambda) * T_{sample}(\lambda) d\lambda \quad \text{Equation 2}$$

if we **assume** the response of the system $R(\lambda)$ is constant from λ_1 to λ_2

$$O_{open\ beam} = C \quad \text{Equation 3}$$

$$O_{sample} = C\left[\int_{\lambda_1}^{\lambda_2} T_{sample}(\lambda) d\lambda\right] \quad \text{Equation 4}$$

For each passband filter, there is a different λ_1, λ_1 and C, but for clarity we are only considering one passband filter at the moment.

The metric chosen, *M*, when utilizing the filtometer has been the output from the detector with the sample in place divided by the output from the detector without the sample in place.

$$M \equiv \frac{O_{sample}}{O_{open\ beam}} \quad \text{Equation 5}$$

$$M \cong \int_{\lambda_1}^{\lambda_2} T_{sample}(\lambda) d\lambda \quad \text{Equation 6}$$

This metric is measured for each of the passband filters.

We can approximate $T_{sample}(\lambda)$ and $T_{passband}(\lambda)$ by measuring them with the FT-IR. In this way, we can arrive at an approximation of *M.*

$$M \equiv \frac{O_{sample[mV]}}{O_{open\ beam[mV]}} \cong \widehat{M} = \frac{C\left[\sum_{\lambda_o}^{\lambda_f} \hat{T}_{sample}(\lambda) * \hat{T}_{passband}(\lambda)\right]}{C\left[\sum_{\lambda_o}^{\lambda_f} \hat{T}_{passband}(\lambda)\right]} \quad \text{Equation 7}$$

To obtain $\hat{T}_{passband}(\lambda)$, each passband filter was placed in the FT-IR and its transmittance measured; the results are shown in Figure 7. An example of $\hat{T}_{sample}(\lambda) * \hat{T}_{passband}(\lambda)$ is illustrated in Figure 8.

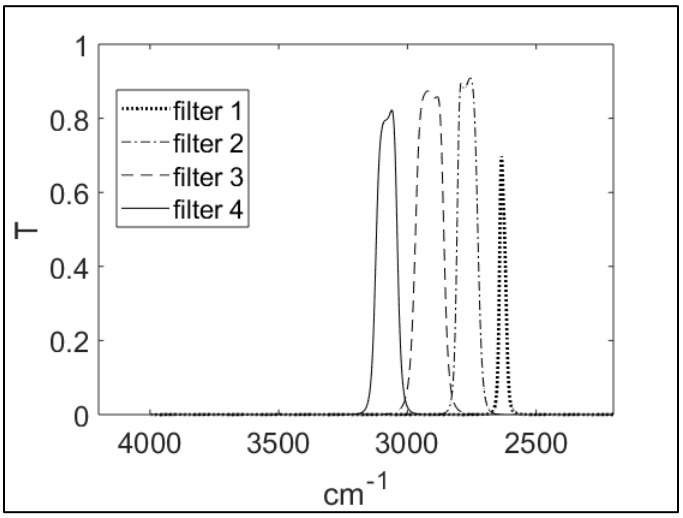

Figure 7. Transmittance of the 5 optical passband filters. Note filter 5 is outside the FT-IR measurement range.

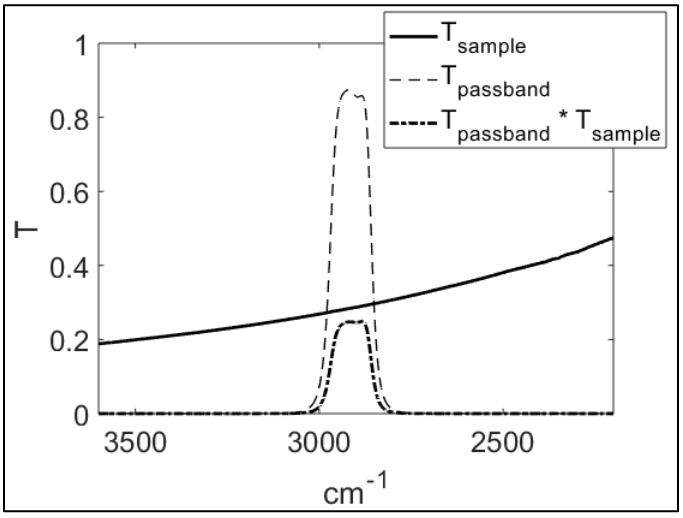

Figure 8. Transmittance of passband filter, a sample (Teflon filter) as measured by FT-IR and their product.